nature chemistry

Article

https://doi.org/10.1038/s41557-023-01363-2

Optical sequencing of single synthetic polymers

Received: 9 February 2023

Accepted: 6 October 2023

Rong Ye[1,2,7], **Xiangcheng Sun**[1,3,7], **Xianwen Mao**[1,4,7], **Felix S. Alfonso**[1], **Susil Baral**[1,5], **Chunming Liu**[1,6], **Geoffrey W. Coates**[1] & **Peng Chen**[1] ✉

Microscopic sequences of synthetic polymers play crucial roles in the polymer properties, but are generally unknown and inaccessible to traditional measurements. Here we report real-time optical sequencing of single synthetic copolymer chains under living polymerization conditions. We achieve this by carrying out multi-colour imaging of polymer growth by single catalysts at single-monomer resolution using CREATS (coupled reaction approach toward super-resolution imaging). CREATS makes a reaction effectively fluorogenic, enabling single-molecule localization microscopy of chemical reactions at higher reactant concentrations. Our data demonstrate that the chain propagation kinetics of surface-grafted polymerization contains temporal fluctuations with a defined memory time (which can be attributed to neighbouring monomer interactions) and chain-length dependence (due to surface electrostatic effects). Furthermore, the microscopic sequences of individual copolymers reveal their tendency to form block copolymers, and, more importantly, quantify the size distribution of individual blocks for comparison with theoretically random copolymers. Such sequencing capability paves the way for single-chain-level structure–function correlation studies of synthetic polymers.

Synthetic polymers are fundamental commodities in modern society[1–3]. Many of them are copolymers, in which various monomers differing in physicochemical properties provide the copolymer tailorable properties[1–4]. The sequence of monomers in copolymers is one crucial factor affecting their properties. Random, alternating, periodic, block and gradient synthetic copolymers can differ drastically in their properties, even with identical monomer compositions and chain lengths[4]. In biological copolymers, such as proteins and nucleic acids, their sequences can uniquely determine the structure/function or genetic information, respectively. Consequently, sequence determination is a key step in understanding the structure–function relations of copolymers.

The sequences of proteins and nucleic acids can be determined at the single-molecule level[5–10], facilitated by the fact that they can be obtained in pure forms, with identical copies, so experimental replications are possible, sequence consensus can be built, and sequence standards can be known. For synthetic copolymers, advanced synthetic approaches have made it possible to control their sequences[4] to encode information[11] or tune their self-assembly behaviour[12], for example. In general, however, synthetic copolymers are highly heterogeneous, with individual chains differing in length, composition and sequence, and their structure–property relationships are only defined at the bulk, averaged level. How the microscopic sequence of a synthetic

---

[1] Department of Chemistry and Chemical Biology, Cornell University, Ithaca, NY, USA. [2] Present address: Department of Chemical Engineering and Catalysis Science and Technology Institute, University of Michigan, Ann Arbor, MI, USA. [3] Present address: Department of Chemical Engineering, Rochester Institute of Technology, Rochester, NY, USA. [4] Present address: Department of Materials Science and Engineering, Institute of Functional Intelligent Materials, and Centre for Advanced 2D Materials, National University of Singapore, Singapore, Singapore. [5] Present address: Department of Chemistry, Illinois State University, Normal, IL, USA. [6] Present address: School of Polymer Science and Polymer Engineering and Department of Chemistry, University of Akron, Akron, OH, USA. [7] These authors contributed equally: Rong Ye, Xiangcheng Sun, Xianwen Mao. ✉ e-mail: pc252@cornell.edu

copolymer determines its properties remains largely unknown. This knowledge gap and the ubiquitous heterogeneity of synthetic polymers call for single-polymer sequencing methods that can resolve and identify individual monomers, preferably in organic solvents where most synthetic polymers are made. Bayley and colleagues have used single-nanopore electrical measurements to track, in real time, the polymerization of single poly(disulfide)s in water at single-monomer resolution[13,14], but the polymer is limited to approximately ten subunits before the nanopore is blocked. Using scanning tunnelling microscopy, Guo and colleagues imaged the polymerization of individual chains of polyethylene of approximately ten subunits on solid surfaces, from gaseous ethylene[15]. We have previously used magnetic tweezers to track single polymer growth in real time in organic solvents, but the resolution was just tens of monomers[16].

In this Article we report the optical sequencing of single synthetic copolymer chains, including in real time for chains with lengths of up to ~10^3 monomers under living polymerization conditions. We achieve this by carrying out multi-colour imaging of polymer growth by single catalysts, at single-monomer resolution and up to sub-micromolar monomer concentrations, using CREATS (coupled reaction approach toward super-resolution-imaging). By coupling a judiciously timed photo-uncaging reaction with the polymerization reaction, CREATS causes the polymerization reaction to be effectively fluorogenic, and the produced fluorescence allows for detection of the inserted monomer and for its single-molecule localization under high reactant concentrations and at a super-optical resolution of tens of nanometres. We find that the chain propagation kinetics of the surface-grafted polymerization shows temporal dynamics and chain-length dependence that are attributable to neighbouring monomer interactions and surface electrostatic effects, respectively, both of which are challenging to assess in bulk polymerization measurements. Moreover, the microscopic sequences of individual copolymers reveal their tendency to form block copolymers instead of random or alternating ones, and, more importantly, quantify the distribution of individual block sizes, which is inaccessible from bulk measurements. Such sequencing capability should pave the way for future structure–function correlation studies of synthetic polymers at the single-chain level.

Results and discussion

CREATS for imaging polymerization

The use of single-molecule fluorescence to image reactions, including polymerizations, has two fundamental requirements[17]: (1) the target fluorescent species needs to be at ultralow concentrations (typically $<10^{-9}$ M) so that individual fluorescent molecules can be spatially separated beyond diffraction-limited resolution (~300 nm) and then imaged; (2) the reactant (for example, the monomer) concentration needs to be sufficiently high to have appreciable reaction kinetics. To satisfy these two requirements, a well-known strategy is to use fluorogenic reactions, in which nonfluorescent reactants can be supplied at high concentrations, but the fluorescent products are few[9,18–23]. Most polymerization reactions cannot be adapted to be fluorogenic, however. Previous single-molecule fluorescence studies of polymerizations have used dye-labelled monomers at a concentration of 10^{-13} to 10^{-9} M mixed with 10^{-3} to 10^{-2} M unlabelled monomers to satisfy these two requirements[24–26]. However, under such conditions, merely 1 out of $>10^6$ inserted monomers were detectable, making the complete polymerization inaccessible. Single-polymer growth at single-monomer resolution is yet to be achieved via fluorescence imaging[17].

We have devised CREATS as a general strategy to render reactions fluorogenic. Figure 1a illustrates CREATS using, as an example, a surface-grafted chain-growth polymerization, a technique that is important for surface modifications in organic electronics and tissue engineering[27,28]. Here, polymerization of monomers is not fluorogenic (Fig. 1a, top left), but another separate reaction is fluorogenic (Fig. 1a, bottom left). By linking the monomer and the pro-fluorescent reactant, we have a coupled reaction, in which the fluorogenic component reports the polymerization reaction (Fig. 1a, right).

We implemented CREATS to study the ring-opening metathesis polymerization (ROMP) catalysed by Grubbs' second-generation-catalyst (**G2**) (Fig. 1a, right and Supplementary Fig. 1a), a widely used reaction for synthesizing polymers with tunable sizes, architectures and functions[29]. The fluorogenic reaction is a photo-uncaging reaction (Fig. 1a, bottom left). The monomer norbornene is coupled to a pro-fluorescent side chain, comprising a BODIPY-based fluorophore that is quenched via photo-induced electron transfer by a caging group (2,6-dinitrobenzyl)[30], whose photo-cleavage restores the fluorescence (Fig. 1a,d–f). During polymerization in a microfluidic reactor, monomers are supplied continuously to achieve steady-state kinetics (Fig. 1c). A laser (375 nm) first uncages the monomers that are inserted into surface-grafted polymers (Fig. 1b, top). After a delay to allow uncaged free monomers to diffuse out of the observation volume, promoted by the solution flow, a second laser is used to image the inserted, immobilized monomers and subsequently bleach them, before the uncaging–imaging–bleaching cycle repeats (Fig. 1b, middle/bottom). All lasers are in total-internal-reflection geometry, where the evanescent field allows for a small observation volume and better background suppression at higher monomer concentrations. The uncaging–imaging–bleaching cycling rate is performed faster than the polymerization rate to capture each monomer during real-time polymerization imaging, where each inserted monomer is imaged and localized at nanometre precision via single-molecule localization microscopy[31–34] (Methods and Supplementary Section 1.1).

We synthesized three norbornene-based monomers (*endo*- and *exo*-mixtures), each carrying a BODIPY-based pro-fluorescent side chain whose uncaged product emits green, yellow or red fluorescence to be differentiable during copolymerization (Fig. 1d–g and Supplementary Sections 1.3 to 1.6). These monomers can be photo-uncaged efficiently (Fig. 1h–i). The green monomer has the highest fluorescence on–off ratio of ~100 (Fig. 1g), and the yellow and red monomers have on–off ratios of ~23 and ~5.9 (the latter is too low for further use), respectively (Supplementary Fig. 33). Neither of these monomers contains functional groups that would interfere with **G2**-catalysed ROMP[35], as confirmed by bulk reaction measurements (Supplementary Sections 2.1.2 and 2.1.4). The 12-atom-long spacer between norbornene and the fluorophore is crucial for their ROMP, as a short three-atom spacer deactivates the monomer, probably due to steric hindrance (Supplementary Section 2.1.1).

We further labelled the **G2** with the green-BODIPY fluorophore (Supplementary Section 1.7) and grafted it onto silica-coated magnetic marker particles (hundreds of nanometres in size and irregular in shape) to be dispersed sparsely in the microfluidic reactor (Fig. 1c,j). The grafting reaction also initiates **G2** for subsequent ROMP reactions (that is, the PCy_3 ligand of **G2** dissociates and is washed away; Supplementary Section 1.2). The magnetic particles facilitate the removal of ungrafted catalysts in an air-free environment (Supplementary Section 1.1) and help locate the catalysts, which can be counted and localized to nanometre precision via single-molecule fluorescence imaging.

Monomer-resolved single-polymer growth

With CREATS, we first studied the homopolymerization of monomer **A** in *n*-hexane under a N_2-protected environment (Methods). The *n*-hexane has a refractive index that is sufficiently lower than that of quartz to readily implement total internal reflection fluorescence (TIRF) microscopy (Methods). A single labelled **G2** on a magnetic marker particle was first imaged, localized to nanometre precision, and then photobleached (Fig. 2a,b and Supplementary Section 2.3.6), in correlation with scanning electron microscopy (SEM) of the marker particle (Supplementary Fig. 35a). Upon flowing the monomer solution into the reactor cell to achieve steady-state polymerization kinetics, we performed uncaging–imaging cycles at 1 cycle per minute to sample

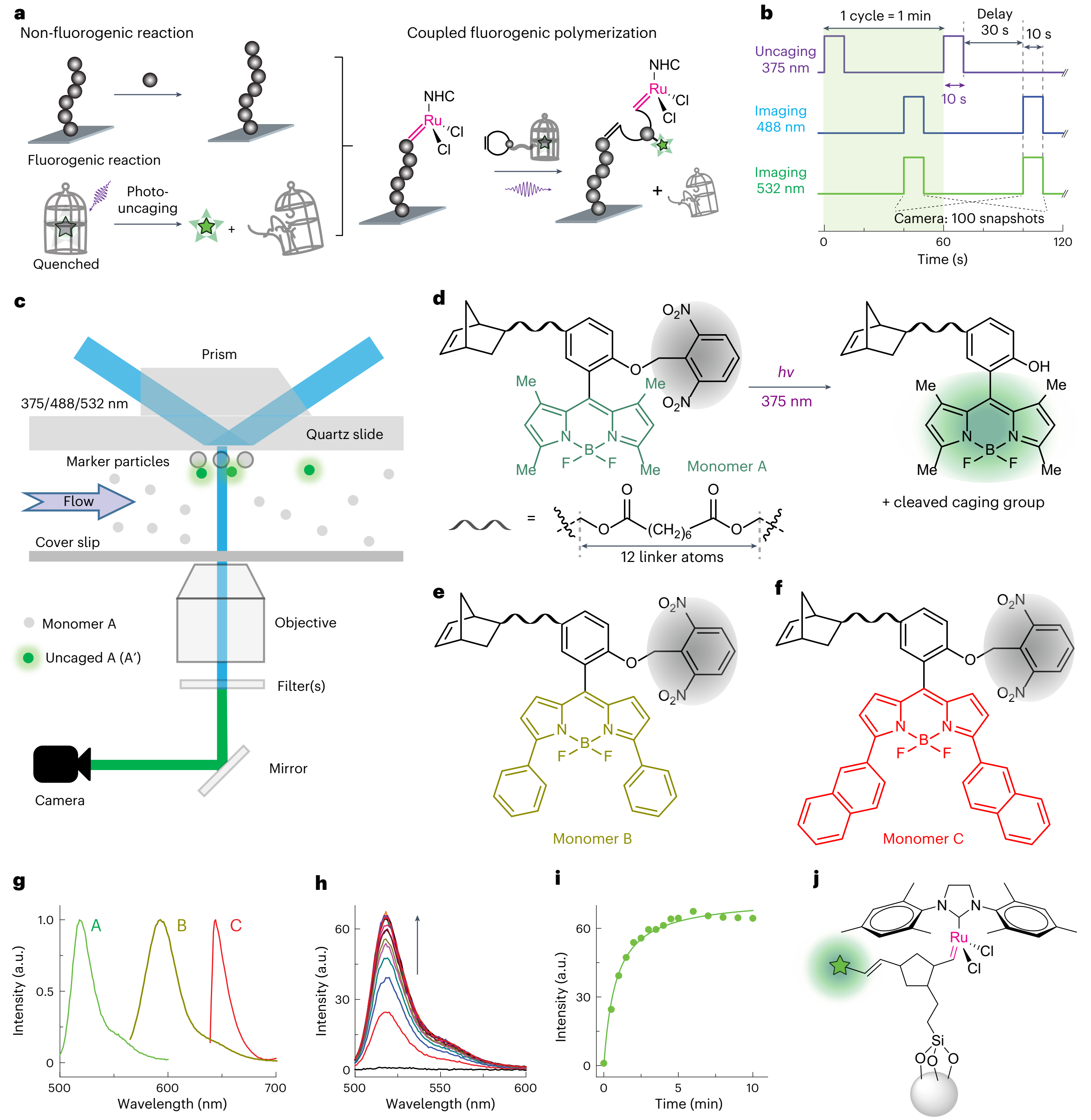

Fig. 1 | CREATS for single-molecule super-resolution imaging of ROMP at high monomer concentrations. **a**, Design of CREATS, illustrated by coupling a surface-grafted chain-growth polymerization reaction (for example, ROMP catalysed by **G2**) and a fluorogenic photo-uncaging reaction, enabling the overall reaction to be effectively fluorogenic for single-molecule super-resolution imaging. NHC, N-heterocyclic carbene. **b**, Laser and camera timing diagram for repeated cycles of uncaging, imaging (two-colour) and bleaching the inserted monomers during polymerization. **c**, Scheme of the experimental set-up for imaging real-time polymerization reactions in operando via TIRF microscopy. **d**–**f**, Structures of three caged monomers (monomer **A** in **d**; monomer **B** in **e**; monomer **C** in **f**) and the uncaging reaction scheme (shown in **d**). Fluorophores are colour-coded by their emission colours. The caging group is shaded in grey. **g**, Fluorescence spectra of monomer **A**, **B** and **C** after photo-uncaging; their limited spectral overlap allows for concurrent detection of different monomers through spectral separation. **h**, Fluorescence spectra of monomer **A** uncaging under 375-nm irradiation (~30 mW cm^{-2}) over time in CHCl$_3$, showing the uncaging process. **i**, Fluorescence intensity at 518 nm versus time from **h**. The line is a fit with saturation function $y = abx/(1 + bx) + c$, with fitting parameters $a = 73 \pm 1$, $b = 1.21 \pm 0.07\ \mathrm{min}^{-1}$ and $c = 0 \pm 1$. **j**, Scheme of green-BODIPY-labelled **G2** after grafting onto a norbornene-functionalized magnetic particle.

the inserted monomers (Fig. 1b). The 375-nm uncaging laser was on for 10 s, giving a photo-uncaging efficiency of ~95% within two cycles (Supplementary Section 2.3.2). After a 30-s delay to allow uncaged free monomers to diffuse away, the 488-nm imaging laser was turned on for 10 s (much longer than the 2.2 ± 0.3 s photobleaching lifetime of the green fluorophore under such imaging conditions; Supplementary Fig. 34d–g), during which fluorescence images were captured continuously (100 ms per frame). A typical fluorescence intensity

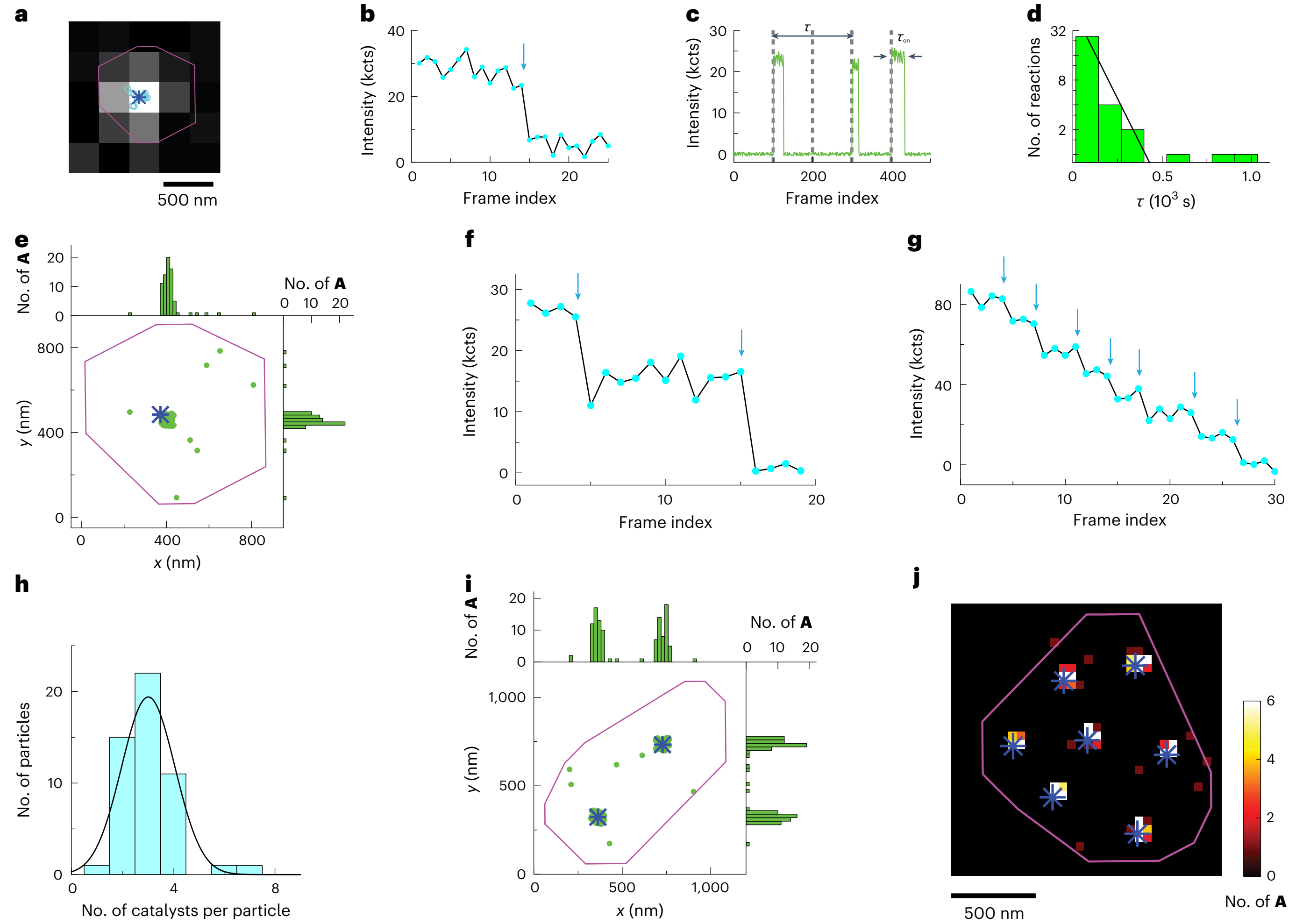

Fig. 2 | Super-resolution imaging of single-polymer growth at single-monomer resolution. a, Fluorescence image of a fluorophore-labelled catalyst on a magnetic marker particle. Purple line: structural contour of the marker particle from SEM, expanded by the image pixel size of ~267 nm (Supplementary Fig. 35a). The circles and asterisk show the locations of the catalyst from each image and from the frame-averaged image, respectively. **b**, Background-subtracted fluorescence intensity trajectory of the labelled catalyst from **a**, showing a single photobleaching step (blue arrow), characteristic of single molecules. **c**, A segment of the background-subtracted fluorescence intensity trajectory during polymerization on the catalyst in **a** at [**A**] = 0.1 μM, showing clear fluorescence-on bursts, where each burst reports an added monomer during polymerization. Vertical dashed lines mark the start of the 488-nm imaging laser. The *x* axis is plotted as the image frame index instead of time because the images were not taken at consistent time intervals due to our cyclic uncaging, delay and imaging scheme (Fig. 1b). **d**, Histogram of *τ* from the catalyst in **a** at [**A**] = 0.1 μM. The *y* axis is in log scale. The solid line is an exponential fit with a time constant of (3.6 ± 0.7) × 10^2 s. **e**, Locations of inserted monomers during polymerization (each green dot represents one monomer), overlaid on the catalyst location (blue asterisk) and the marker particle contour (purple line) from **a**. Top and right: one-dimensional histograms of the monomer locations; their spatial dispersion around the catalyst is ~49 nm (full-width at half-maximum of the Gaussian fit; Supplementary Fig. 25q). **f**,**g**, Same as in **b**, but for two marker particles carrying two (**f**) and seven (**g**) catalysts, respectively. Each arrow marks one photobleaching step, so the number of arrows indicates the number of catalysts. **h**, Histogram of catalyst counts per marker particle. The solid line is a Gaussian fit centred at 3.0 ± 0.1. **i**, As in **e**, but for the two catalysts in **f**. **j**, Two-dimensional histogram of the monomer locations overlaid on the catalyst positions and marker particle contour for the seven catalysts in **g**. Bin size: 50 × 50 nm^2. The spatial dispersion of the monomers around each catalyst position is ~22–61 nm in **i** and **j** (Supplementary Fig. 25r).

trajectory from a single catalyst shows on–off bursts of fluorescence during polymerization, with fluorescence-on levels at the expected intensity for individual monomer insertion events (Fig. 2c). The fluorescence-on time (τ_{on}) also follows an exponential distribution and averages at 2.2 ± 0.1 s, as expected for single fluorophore photobleaching (Supplementary Fig. 34d–g). Moreover, not every imaging cycle detected a monomer (Fig. 2c), consistent with the stochastic nature of single-molecule reaction kinetics[22,36]. The time separation *τ* from one burst to the next is the microscopic monomer reaction time, and $\langle\tau\rangle^{-1}$, where ⟨ ⟩ denotes averaging, is the turnover frequency (TOF) of the catalyst. Furthermore, the distribution of *τ*, either from a single catalyst (Fig. 2d) or compiled from many catalysts (Supplementary Fig. 35d), follows a single exponential, indicating that the underlying polymerization kinetics contains a single rate-limiting step under our reaction conditions.

The single-monomer resolution also allowed for nanometre-level localization of the individual polymerized monomers. They cluster around the catalyst position on the marker particle (Fig. 2e), further supporting that they were polymerized on the same chain by a single catalyst. At [**A**] = 2 nM, the TOF is (4 ± 3) × 10^{-5} s^{-1} per catalyst, averaged from many catalysts (Supplementary Fig. 35e) (the error bar here is the standard deviation among individual catalysts, reflecting the dispersion). In contrast, control analyses on marker particles without catalysts give an apparent rate of insignificant value (<2.5 × 10^{-6} s^{-1} per particle; Supplementary Fig. 35g). Fluorescence bursts are also detected off the marker particles, which are attributable mostly to nonspecific adsorption of uncaged free monomers onto the surface (or sometimes noise-induced false detections); the detection frequency for these is negligible compared with the on-catalyst TOFs (Supplementary Fig. 35h and Supplementary Section 2.4.6). Moreover, $\langle\tau_{\mathrm{on}}\rangle$ for the off-particle events is 1.0 ± 0.1 s (Supplementary Fig. 35j), notably shorter than that for the on-catalyst events, which is expected for nonspecifically adsorbed monomers, which can undergo desorption in addition to photobleaching. Additional control experiments using optical imaging, SEM imaging and deactivated **G2** catalyst further support that polymers can indeed grow on the **G2**-decorated marker particles and the detected monomers on these particles are not due to monomer aggregation or physisorption (Supplementary Section 2.2).

Most marker particles contain multiple catalysts (Fig. 2h). The number of catalysts and their locations can be determined from catalyst-label fluorescence photobleaching steps and corresponding imaging localizations (Fig. 2f–g; Supplementary Section 1.8 provides details about the catalyst localization analysis). On such marker particles, the positions of polymerized monomers display discrete nanosized clusters, each around a single catalyst (Fig. 2i,j). Such super-resolved multi-catalyst cases demonstrate the power of imaging single-polymer growth at single-monomer resolution.

Growth kinetics and dynamics

Imaging single-catalyst polymerization in real time at single-monomer resolution immediately enabled us to determine the single-chain polymerization kinetics. Using CREATS, we titrated [**A**] to 0.1 µM (orders of magnitude higher than used in previous single-molecule fluorescence studies of polymerization reactions[24]), growing individual polymers to up to >10^2 subunits, with dispersion $Đ = 1.36$ (Supplementary Fig. 35f and Supplementary Section 2.4.4). The TOF is linear with respect to [**A**] at both the single-catalyst/polymer level and on average (Fig. 3a), as expected for first-order kinetics with respect to the monomer for ROMP at nanomolar to micromolar monomer concentrations[16,37], where monomer binding is rate-limiting in the chain-propagation kinetics (that is, step k_{II} in Supplementary Fig. 1a). The overall second-order rate constant $k_{\mathrm{II}}^{\mathrm{A}}$ of individual polymers (including the first order with respect to the catalyst concentration) follows an approximately log-normal distribution, averaging at $(6 \pm 1) \times 10^3\ \mathrm{M^{-1}\,s^{-1}}$ (Fig. 3c), reflecting the well-known kinetic dispersion of synthetic polymers, and here quantified at the single-polymer level. Similar first-order kinetics with respect to the monomer concentration is also observed for monomer **B**, with its $k_{\mathrm{II}}^{\mathrm{B}}$ averaging at $(7 \pm 2) \times 10^3\ \mathrm{M^{-1}\,s^{-1}}$ (Fig. 3b,d) and possessing comparable reactivity to **A**. Both $k_{\mathrm{II}}^{\mathrm{A}}$ and $k_{\mathrm{II}}^{\mathrm{B}}$ are also consistent with the values deduced from analyses of chain propagation kinetics from bulk homopolymerization of monomers **A** and **B** (Supplementary Section 2.1).

The surface-grafted polymerization described here also enables us to examine surface effects in the polymerization kinetics, which is challenging to study at the bulk level due to kinetic dispersion. Strikingly, at each monomer concentration, the single-catalyst TOF shows a clear dependence on the polymerization degree (that is, chain length), initially increases and eventually saturates to a rate that is substantially larger (Fig. 3e). (Note that at the same polymerization degree or upon extrapolating to zero or infinite polymerization degree, first-order kinetics with respect to the monomer still holds; Supplementary Fig. 36c–g.) $L_{1/2}$, the polymerization degree where the TOF is halfway towards saturation, is ~270 monomers, corresponding to an end-to-end distance of ~15–23 nm (Supplementary Section 2.5.2); this distance is comparable to the ~30 nm Bjerrum length in *n*-hexane (Supplementary Section 2.5.5), at which electrostatic interactions between point charges are comparable to the thermal energy[38]. Similar behaviours were observed for monomer **B** polymerization (Supplementary Fig. 38b,c). Therefore, this polymerization-degree-dependent polymerization kinetics possibly stems from the influence of surface electrostatics, a ubiquitous surface property that could broadly affect surface-grafted polymerizations.

The single-monomer-resolution polymerization trajectories also allow for analysing the autocorrelation function of the microscopic reaction time τ versus the monomer index to evaluate time-dependent dynamics[36]. At [**A**] = 0.1 µM, this autocorrelation, averaged over many polymers to be statistically significant, shows a clear exponential decay with a time constant of 2 ± 1 turnovers, a behaviour that is indiscernible for randomized τ sequences (Fig. 3f). Such autocorrelation reflects a temporal memory effect in polymer growth (that is, dynamic disorder in kinetics[36]), where an earlier faster monomer incorporation tends to be followed by two faster incorporations. Moreover, at lower [**A**] where monomer binding to the catalyst is even more rate-limiting, the autocorrelation amplitude becomes indiscernible (Supplementary Fig. 37), suggesting that this memory effect originates more from monomer insertion than from monomer binding in the catalytic cycle (that is, k_{III} versus k_{II} step, Supplementary Fig. 1a). Such temporal dynamics, observed also for monomer **B** (Supplementary Fig. 38d) and inaccessible from bulk polymerization studies, suggests that underlying dynamic processes (for example, intra-chain neighbouring monomer interactions) could modulate polymerization kinetics on surfaces or in solution (Supplementary Section 2.6.2).

Single copolymer sequencing

Having imaged single-catalyst polymerization at single-monomer resolution with monomer **A** or **B**, we proceeded to sequence single polymers during copolymerization. We used 488- and 532-nm lasers to excite the uncaged **A** and **B** simultaneously for two-colour imaging (Fig. 1b and Methods). At a molar ratio of **A**:**B** = 1:1 with a total monomer concentration of 0.1 µM, the polymerized **A** and **B** monomers cluster together at the same catalyst (Fig. 4a), consistent with their copolymerization. In the corresponding single-catalyst copolymerization fluorescence trajectories (Fig. 4b), the colour of inserted monomers immediately reports the copolymer sequence. We sequenced many tens of copolymers (Fig. 4c), and their lengths follow an approximately log-normal distribution, up to ~10^3 subunits long (Fig. 4d). The average monomer composition is 1:1 (Fig. 4e), as expected from the comparable ROMP reactivity of **A** and **B**.

No other methods exist to sequence such synthetic copolymers individually, a long-standing unmet need in the field[39]. Therefore, to further test our method, we varied the ratio and total concentration of the two monomers. The average compositions of the sequenced copolymers directly follow the ratios of the monomers (Fig. 4e), and the single-catalyst TOF also scales linearly with the total monomer concentration (Fig. 4f). Both results support our sequencing fidelity. Additional control experiments using the two-colour imaging protocol further support our sequencing fidelity (Supplementary Section 3.1): (1) under homopolymerization of monomer **A** or **B**, only the corresponding monomer is detected, but not the other; (2) switching the reactant supply from one monomer to the other in the middle of a homopolymerization reaction is accompanied by a concurrent change in the detected monomer; (3) during copolymerization, replacing the green monomer **A** by its inactive analogue, which has a short linker, abolishes signal detection in the green channel. We further performed statistical analyses considering possible errors from missed detection, mis-identification and mis-ordering, and the overall fidelity of detecting each monomer in the sequencing was estimated to be ~90%, which could be further improved in the future using more photostable and brighter fluorophores[40] (Supplementary Section 3.2).

The single-catalyst copolymerization fluorescence trajectories also resolve four different microscopic monomer reaction times—τ_{AA}, τ_{AB}, τ_{BB} and τ_{BA}—which depend on the identity of the incorporated monomer and the preceding one in the growing chain (Fig. 4b). All follow single-exponential distributions as expected, but with clearly different decay constants (Fig. 4g). The corresponding four rate constants differ

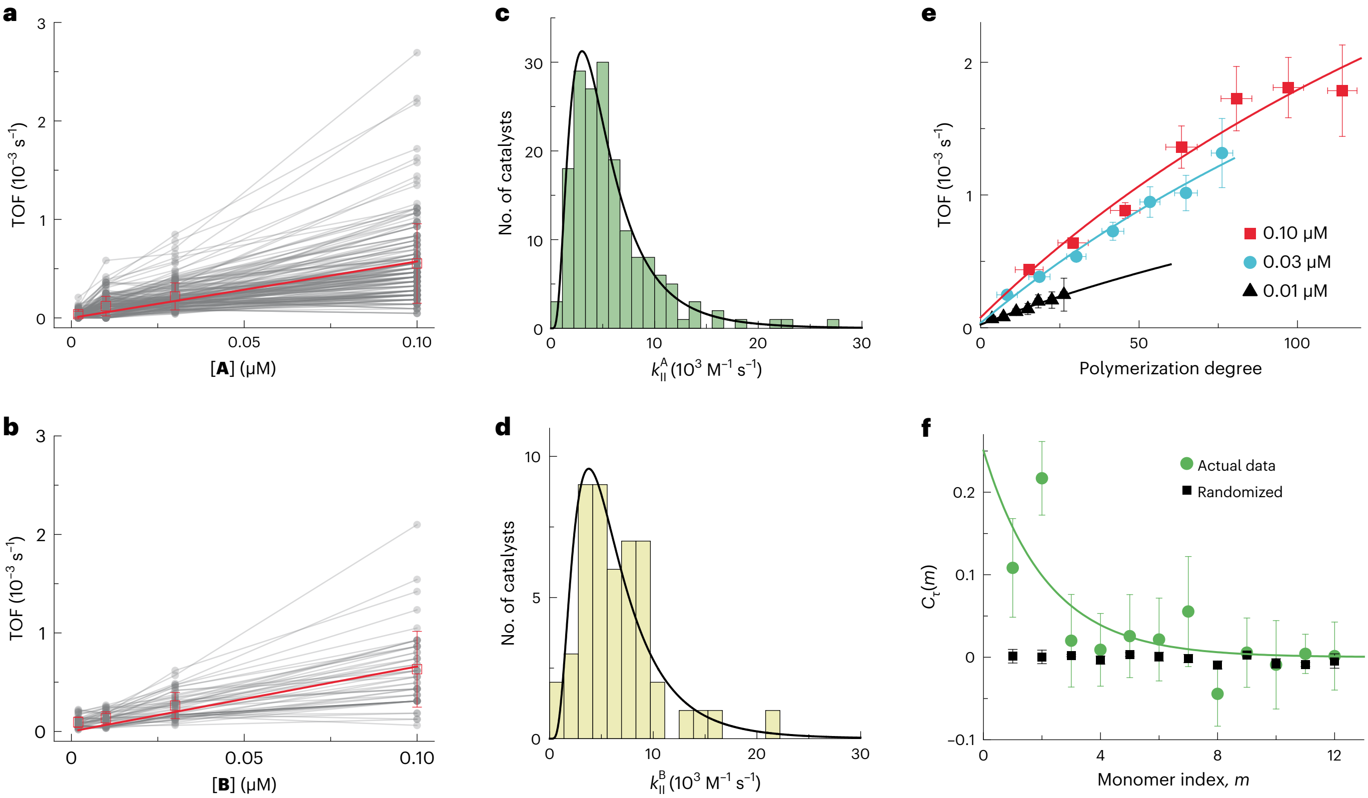

Fig. 3 | Single-catalyst polymerization kinetics and dynamics at single-monomer resolution. a,**b**, Single-catalyst TOF versus monomer concentration [**A**] (**a**) and [**B**] (**b**). Grey dots and lines represent individual catalysts. Red squares indicate the average of 174 (**a**) and 49 (**b**) catalysts. Red lines are linear fits showing first-order kinetics with respect to monomer concentrations. **c**,**d**, Histograms of single-catalyst rate constants for monomers **A** (**c**) and **B** (**d**) from **a**,**b**. Lines are log-normal fits centred at 5.8 × 10^3 and 6.7 × 10^3 with standard deviations of 4.2 × 10^3 and 3.9 × 10^3 M^{-1} s^{-1}, respectively. **e**, Single-catalyst TOF versus the polymerization degrees for monomer **A**. Lines are global fits with a saturation function $y = ax/(x + L_{1/2}) + c$ with shared $L_{1/2}$ (= 270 ± 50 monomers), which is the polymerization degree where the TOF is halfway towards saturation. **f**, Green circles represent the autocorrelation function of microscopic reaction time τ, $C_\tau(m) = \langle \Delta\tau(0)\Delta\tau(m)\rangle/\langle \Delta\tau^2\rangle$ (ref. 36), where m is the index of monomer **A** (0.1 μM) insertions in the single-catalyst polymerization trajectory, $\Delta\tau(m) = \tau(m) - \langle\tau\rangle$, and $\langle\ \rangle$ denotes averaging. $C_\tau(m)$ here is weight-averaged based on the trajectory lengths from 14 catalysts showing ≥20 turnovers of **A**. The green line is an exponential fit, with amplitude of 0.25 ± 0.03 and time constant of 2 ± 1. Black squares represent $C_\tau(m)$ from randomized τ sequences. N is 174 in **a**,**f** and 49 in **b**. Error bars represent s.d. in **a**, **b** and **e**, and s.e.m. in **f**, with the mean at the centre in all plots. The sample size of data points in **e** varies (see Supplementary Fig. 36 for details).

accordingly (Fig. 4h), indicating that a preceding monomer affects the polymerization kinetics of the next, consistent with our earlier observation of a temporal memory effect in polymerization dynamics (Fig. 3f). The two reactivity ratios, r_1 (= k_{AA}/k_{AB}) and r_2 (= k_{BB}/k_{BA}), can qualitatively predict the copolymer sequence patterns, which can usually be estimated from bulk measurements (Supplementary Section 2.8.1)[41,42]. Both ratios here are >1 ($r_1 = 1.7$ and $r_2 = 1.5$), consistent with those extracted from bulk copolymerization kinetics (Supplementary Section 2.1.7) and reflecting a tendency to chain propagation of the same monomer during copolymerization to form blocks. We therefore examined the microscopic sequence patterns in the individual 1:1 copolymers, which we measured over an extended reaction time (>48 h) to obtain long copolymer chains. Compared with the simulated random copolymers, which also have continuous block segments whose size distribution follows $x/2^x$ scaling (Supplementary Section 2.8.2), the experimentally observed **A** (or **B**) blocks show clearly higher occurrences for larger blocks (Fig. 4i), quantifying the qualitative prediction from the reactivity ratios.

We further analysed the conditional probabilities of the sequence fragments (Supplementary Section 2.8.3), that is, the probability of the last monomer given the previous sequence in the fragment. For single-subunit fragments, the overall probability for either **A** or **B** is 0.5, as expected for 1:1 copolymers (Fig. 4j). For **XX** fragments (**X** = **A** or **B**), the conditional probability is significantly higher than 0.5 for simulated random copolymers (Fig. 4j). More importantly, this higher conditional probability is more pronounced for **XXX** fragments and then plateaus towards longer blocks—it reaches ~90% of the plateau at approximately four-monomer blocks, quantifying the tendency of forming longer blocks in these copolymers. Moreover, the conditional probabilities for alternating fragments like **XY** and **XYXY** are significantly lower than those for random copolymers (Fig. 4j). Taken together (Supplementary Section 2.8.4), these copolymers tend to form homo-blocks that are approximately four monomers longer than those in completely random copolymers.

Conclusions

We have developed CREATS for imaging single-catalyst polymerization at single-monomer resolution, in real time and at high reactant concentrations. Besides ROMP, CREATS is applicable to any chain-growth polymerizations, including living anionic polymerization, living cationic polymerization, living free radical polymerization, and living chain-growth polycondensations, in which the monomers could also be varied in structure and size (Supplementary Section 4.2), and here it enabled us to quantify the effects of surface-grafting on polymerization kinetics and uncover the temporal dynamics of single-chain growth. The knowledge derived here has the potential to impact the

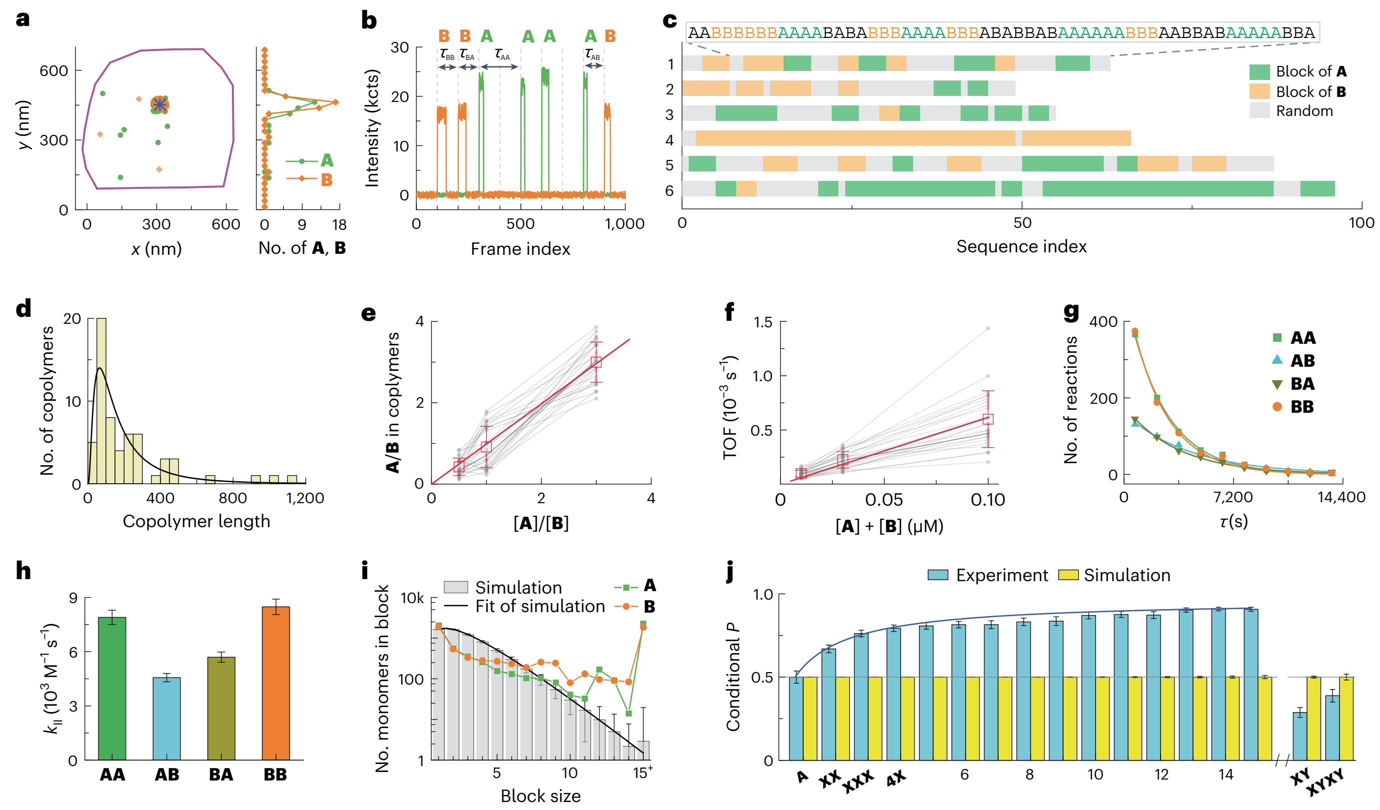

Fig. 4 | Single copolymer sequencing. a, Locations of individual polymerized monomer **A** (green dots) and **B** (yellow dots) around a single labelled **G2** (blue asterisk) at **A**:**B** = 1:1. The purple line is the expanded contour of the magnetic marker particle from its SEM image (Supplementary Fig. 41 presents more examples). **b**, A segment of the background-subtracted two-colour fluorescence intensity trajectory on the catalyst in **a**, showing the sequence of the grown copolymer. The vertical dashed lines show the start of the 488- and 532-nm imaging lasers. **c**, Sequences of six example copolymers at **A**:**B** = 1:1. Green and yellow blocks denote blocks of three or more **A** and **B** subunits, respectively, and the other sequence patterns are in grey. Copolymer **1** is from **a** and **b**. More sequences are provided in Supplementary Table 2. **d**, Length distribution of 60 sequenced copolymers. **e**, Grey lines show the ratio of the **A**/**B** subunits in the individual sequenced copolymers versus the supplied **A**/**B** monomer concentration ratio. Red open squares show the averaged results. The red line is the diagonal. **f**, Single-catalyst TOF versus total monomer concentrations for 25 catalysts. Red open squares show averaged results. The red line is a linear fit. **g**, Distributions of four different microscopic monomer reaction times τ during copolymerization at [**A**] = [**B**] = 0.05 μM. Solid lines show exponential fits, whose decay constants give rates r_{AA}, r_{AB}, r_{BA} and r_{BB} of 0.00039 ± 0.00001, 0.00023 ± 0.00001, 0.00028 ± 0.00001 and 0.00042 ± 0.00002 s^{-1}, respectively. **h**, Rate constants of the four chain-propagation reactions, giving reactivity ratios $r_1 = k_{AA}/k_{AB} = 1.7$ and $r_2 = k_{BB}/k_{BA} = 1.5$. **i**, Distribution of the observed total number of **A** or **B** monomers in different block sizes in comparison with that of the simulated random copolymers at **A**:**B** = 1:1 (Supplementary Section 2.8.2). The black line is a fit with $y = Cx/2^x$, where C is a constant. The last bin represents blocks of 15 and larger. **j**, Conditional probability P of sequence fragments extracted from the data of 1:1 copolymers and from simulations of random copolymers (averaged from 1,000 sets) of the same **A**:**B** ratio (Supplementary Section 2.8.3). **X**, **Y** = **A** or **B**; **XX** = **AA** or **BB**; and so on. The blue line is a saturation fit, based on $f(x) = \frac{a(x-1)}{(x-1)+b} + 0.5$, so that $f(1) = 0.5$ is guaranteed; $a = 0.43 \pm 0.01$ and $b = 1.6 \pm 0.1$, where b is the value at which the conditional probability is halfway towards saturation. N is 25 in **e** and **f**, 1,000 (simulations) in **i** and **j**, and 60 (experimental) in **j**. Error bars represent s.d. in **e**, **f** and **i**, 95% fitting confidence in **h**, and s.e.m. in **j**, with the mean at the centre in all plots.

field of polymer synthesis by helping the design and optimization of surface-grafting polymerization conditions (for example, by unravelling the intricate connection between polymer length and reaction kinetics) and of copolymerization reaction conditions (for example, by leveraging insights gained from the resulting copolymer sequence pattern). Furthermore, the microscopic sequences of individual copolymer chains revealed by CREATS not only map the sequence patterns of synthetic copolymers, but also enable future structure–function correlation studies at the single-chain level, for example in coupling to magnetic tweezers measurements on single-chain mechanics[16] or as structural inputs for molecular dynamics simulations of polymer chains[43].

Online content

Any methods, additional references, Nature Portfolio reporting summaries, source data, extended data, supplementary information, acknowledgements, peer review information; details of author contributions and competing interests; and statements of data and code availability are available at https://doi.org/10.1038/s41557-023-01363-2.

References

1. Odian, G. In *Principles of Polymerization* 1–38 (Wiley, 2004).
2. Korley, L. T. J., Epps, T. H., Helms, B. A. & Ryan, A. J. Toward polymer upcycling-adding value and tackling circularity. *Science* **373**, 66–69 (2021).
3. Urban, M. W. et al. Key-and-lock commodity self-healing copolymers. *Science* **362**, 220–225 (2018).
4. Lutz, J.-F., Ouchi, M., Liu, D. R. & Sawamoto, M. Sequence-controlled polymers. *Science* **341**, 1238149 (2013).
5. Harris, T. D. et al. Single-molecule DNA sequencing of a viral genome. *Science* **320**, 106–109 (2008).

6. Eid, J. et al. Real-time DNA sequencing from single polymerase molecules. *Science* **323**, 133–138 (2009).
7. Alfaro, J. A. et al. The emerging landscape of single-molecule protein sequencing technologies. *Nat. Methods* **18**, 604–617 (2021).
8. Restrepo-Pérez, L., Joo, C. & Dekker, C. Paving the way to single-molecule protein sequencing. *Nat. Nanotechnol.* **13**, 786–796 (2018).
9. Sims, P. A., Greenleaf, W. J., Duan, H. & Xie, X. S. Fluorogenic DNA sequencing in PDMS microreactors. *Nat. Methods* **8**, 575–580 (2011).
10. Reed, B. D. et al. Real-time dynamic single-molecule protein sequencing on an integrated semiconductor device. *Science* **378**, 186–192 (2022).
11. Dahlhauser, S. D. et al. Molecular encryption and steganography using mixtures of simultaneously sequenced, sequence-defined oligourethanes. *ACS Cent. Sci.* **8**, 1125–1133 (2022).
12. Bazzi, H. S., Bouffard, J. & Sleiman, H. F. Self-complementary ABC triblock copolymers via ring-opening metathesis polymerization. *Macromolecules* **36**, 7899–7902 (2003).
13. Shin, S.-H. & Bayley, H. Stepwise growth of a single polymer chain. *J. Am. Chem. Soc.* **127**, 10462–10463 (2005).
14. Pulcu, G. S. et al. Single-molecule kinetics of growth and degradation of cell-penetrating poly(disulfide)s. *J. Am. Chem. Soc.* **141**, 12444–12447 (2019).
15. Guo, W. et al. Visualization of on-surface ethylene polymerization through ethylene insertion. *Science* **375**, 1188–1191 (2022).
16. Liu, C. et al. Single polymer growth dynamics. *Science* **358**, 352–355 (2017).
17. Liu, C. et al. Real-time single-polymer growth towards single-monomer resolution. *Trends Chem.* **3**, 318–331 (2021).
18. Edman, L., Földes-Papp, Z., Wennmalm, S. & Rigler, R. The fluctuating enzyme: a single molecule approach. *Chem. Phys.* **247**, 11–22 (1999).
19. Flomenbom, O. et al. Stretched exponential decay and correlations in the catalytic activity of fluctuating single lipase molecules. *Proc. Natl Acad. Sci. USA* **102**, 2368–2372 (2005).
20. English, B. P. et al. Ever-fluctuating single enzyme molecules: Michaelis–Menten equation revisited. *Nat. Chem. Biol.* **2**, 87–94 (2006).
21. Roeffaers, M. B. J. et al. Spatially resolved observation of crystal-face-dependent catalysis by single turnover counting. *Nature* **439**, 572–575 (2006).
22. Xu, W., Kong, J. S., Yeh, Y.-T. E. & Chen, P. Single-molecule nanocatalysis reveals heterogeneous reaction pathways and catalytic dynamics. *Nat. Mater.* **7**, 992–996 (2008).
23. Naito, K., Tachikawa, T., Fujitsuka, M. & Majima, T. Real-time single-molecule imaging of the spatial and temporal distribution of reactive oxygen species with fluorescent probes: applications to TiO_2 photocatalysts. *J. Phys. Chem. C* **112**, 1048–1059 (2008).
24. Easter, Q. T. & Blum, S. A. Single turnover at molecular polymerization catalysts reveals spatiotemporally resolved reactions. *Angew. Chem. Int. Ed.* **56**, 13772–13775 (2017).
25. Yu, D., Garcia, A. I. V., Blum, S. A. & Welsher, K. D. Growth kinetics of single polymer particles in solution via active-feedback 3D tracking. *J. Am. Chem. Soc.* **144**, 14698–14705 (2022).
26. Eivgi, O. & Blum, S. A. Exploring chemistry with single-molecule and -particle fluorescence microscopy. *Trends Chem.* **4**, 5–14 (2022).
27. Wang, S. et al. Surface-grafting polymers: from chemistry to organic electronics. *Mater. Chem. Front.* **4**, 692–714 (2020).
28. Barbey, R. et al. Polymer brushes via surface-initiated controlled radical polymerization: synthesis, characterization, properties and applications. *Chem. Rev.* **109**, 5437–5527 (2009).
29. Bielawski, C. W. & Grubbs, R. H. Living ring-opening metathesis polymerization. *Prog. Polym. Sci.* **32**, 1–29 (2007).
30. Kobayashi, T. et al. Highly activatable and environment-insensitive optical highlighters for selective spatiotemporal imaging of target proteins. *J. Am. Chem. Soc.* **134**, 11153–11160 (2012).
31. Yildiz, A. & Selvin, P. R. Fluorescence imaging with one nanometer accuracy: application to molecular motors. *Acc. Chem. Res.* **38**, 574–582 (2005).
32. Betzig, E. et al. Imaging intracellular fluorescent proteins at nanometer resolution. *Science* **313**, 1642–1645 (2006).
33. Rust, M. J., Bates, M. & Zhuang, X. Sub-diffraction-limit imaging by stochastic optical reconstruction microscopy (STORM). *Nat. Methods* **3**, 793–796 (2006).
34. Su, L. et al. Super-resolution localization and defocused fluorescence microscopy on resonantly coupled single-molecule, single-nanorod hybrids. *ACS Nano* **10**, 2455–2466 (2016).
35. Vougioukalakis, G. C. & Grubbs, R. H. Ruthenium-based heterocyclic carbene-coordinated olefin metathesis catalysts. *Chem. Rev.* **110**, 1746–1787 (2010).
36. Lu, H. P., Xun, L. & Xie, X. S. Single-molecule enzymatic dynamics. *Science* **282**, 1877–1882 (1998).
37. Sanford, M. S., Love, J. A. & Grubbs, R. H. Mechanism and activity of ruthenium olefin metathesis catalysts. *J. Am. Chem. Soc.* **123**, 6543–6554 (2001).
38. Moritz, R. et al. Ion size approaching the bjerrum length in solvents of low polarity by dendritic encapsulation. *Macromolecules* **47**, 191–196 (2014).
39. Mutlu, H. & Lutz, J.-F. Reading polymers: sequencing of natural and synthetic macromolecules. *Angew. Chem. Int. Ed.* **53**, 13010–13019 (2014).
40. Grimm, J. B. et al. Bright photoactivatable fluorophores for single-molecule imaging. *Nat. Methods* **13**, 985–988 (2016).
41. Lin, T.-P. et al. Control of grafting density and distribution in graft polymers by living ring-opening metathesis copolymerization. *J. Am. Chem. Soc.* **139**, 3896–3903 (2017).
42. Chang, A. B. et al. Design, synthesis and self-assembly of polymers with tailored graft distributions. *J. Am. Chem. Soc.* **139**, 17683–17693 (2017).
43. Hilburg, S. L., Ruan, Z., Xu, T. & Alexander-Katz, A. Behavior of protein-inspired synthetic random heteropolymers. *Macromolecules* **53**, 9187–9199 (2020).

Methods

Synthesis and characterization of monomers and labelled catalyst

All reagents and solvents (ACS grade) were purchased through Sigma-Aldrich, Fisher Scientific or Alfa Aesar and used without purification. All solvents were used without drying unless otherwise indicated. The solvents *n*-hexane and toluene involved in single-molecule imaging were dried and stored under a nitrogen atmosphere after purchase, then further photobleached before use. Details are provided in Supplementary Section 1.1.

The caged monomers and the labelled Grubbs second-generation catalyst were synthesized in house and structurally characterized by ^{1}H NMR, ^{13}C NMR and/or MS. Detailed synthesis procedures and the characterizations of compounds are provided in Supplementary Sections 1.6 and 1.7. The photo-uncaging properties of the caged monomers and the photobleaching properties of the uncaged monomers were characterized at both the ensemble and single-molecule level, as described in Supplementary Section 2.3.2–2.3.4. The labelled Grubbs second-generation catalyst was subsequently grafted onto silica-coated magnetic particles (SS0201 Super Mag Silica Beads, Ocean NanoTech), as described in Supplementary Section 1.7. Due to the air-sensitivity of **G2** in liquid, we handled it in a glovebox to prevent its deactivation. Once **G2** was immobilized onto the magnetic particles, we performed washing and separation steps in a glovebox, in which the magnetic property of the particles allowed for pouring out the liquid phase while using a magnet to hold the particles, facilitating handling in the glovebox.

Analytical thin-layer chromatography (TLC) was performed on glass plates coated with silica (60, F_{254}, EMD Chemicals). Visualization was performed with a 254-nm ultraviolet lamp. Column chromatography was carried out with silica gel (60–200 µm, 60A) from Acros Organics. The ^{1}H and ^{13}C NMR spectra were recorded at room temperature on a Varian Inova 400 system (400 MHz) or a Bruker Advance 500 (500 MHz) in $CDCl_3$ solution, and chemical shifts were referenced with the residual proton (7.26 ppm) or carbon (77.16 ppm) signal of the deuterated solvent. High-resolution MS analyses were performed on a Thermo Scientific Exactive Orbitrap MS system equipped with an electrospray ionization source (ESI-HRMS) or with an Ion Sense DART ion source (DART-HRMS). A Zeiss Gemini 500 scanning electron microscope operated at 4 keV at CCMR was used to capture SEM images.

Solvent photobleaching

The organic solvents (for example, *n*-hexane and toluene) used for imaging experiments were irradiated under blue light-emitting diodes (Blue LED Tape Light, 24 V, FLX-00136, PLT Solutions) for at least 24 h to photobleach potential fluorescence impurities[44,45] (Supplementary Fig. 1e). This treatment lowers the background in fluorescence imaging.

Single-molecule fluorescence imaging experiments and data analysis

All single-molecule fluorescence microscopy experiments were carried out on a home-built prism-type wide-field microscope (Olympus IX71) in TIRF geometry. A flow reactor cell (100 µm (height) × 3–5 cm (length) × 1 cm (width)), formed by sandwiching a quartz slide (Technical Glass, drop cast with fluorescent nanodiamonds (NV, ADAMAS NANO) for drift correction and dried), with epoxy glue with minimal double-sided tape for spacing, and a borosilicate coverslip (Gold Seal), was used for in operando imaging.

The catalysts on marker particles were introduced into the flow cell in toluene, washed with *n*-hexane, and then imaged/photobleached. Monomer **A** and/or **B** at 1 nM to 0.1 µM in *n*-hexane under N_2 protection (a positive pressure of N_2 was maintained by a balloon filled with N_2 connected to the monomer solution reservoir) was supplied steadily at ~2 µl min^{-1} to probe the real-time polymerization kinetics. The refractive index of *n*-hexane[46] is 1.375, suitable for TIRF imaging with a quartz prism and quartz slide, as the refractive index of quartz[46] is 1.458. Depending on the amount of data needed for statistical significance, one round of successful imaging experiments typically takes three to five days due to the relatively low polymerization rates under the measured monomer concentrations. The reaction solvent *n*-hexane provides several technically advantageous features: it has a refractive index of 1.37, sufficiently lower than quartz's refractive index of 1.54 for ready implementation of TIRF microscopy; it is not too volatile for maintaining a stable monomer concentration in a long imaging experiment; it does not bind to the Ru centre of the **G2** catalysts; and it is compatible with the epoxy glue that was used to seal the flow cell.

A continuous-wave circularly polarized laser beam was focused onto the sample (~60 × 100 µm^2) in the flow cell to directly photo-uncage the monomers (10.0 mW at 375 nm) or to image and photobleach the uncaged monomers (~33.0 mW at 488 nm for monomer **A** or 12.9 mW at 532 nm for monomer **B**). The timing for the uncaging and imaging lasers is shown in Fig. 1b. The fluorescence emitted by the product was collected by a ×60 NA 1.2 water-immersion objective (UPLSAPO60XW, Olympus), filtered (in single-colour imaging: ET525/50 m, Chroma for 488-nm illumination or HQ580m60, Chroma for 532-nm illumination), and detected by a back-illuminated ANDOR iXon electron-multiplying charge-coupled device (EMCCD) camera (DU897D-CS0-#BV) operated at a frame time of 100-ms. Both 488-nm and 532-nm lasers were used in two-colour imaging experiments (Supplementary Fig. 1c), and the emitted light passed through a Photometrics DV2 two-channel imaging system (Supplementary Fig. 1d), which contained a notch filter (ZET532TopNotch) and a dichroic beamsplitter (FF560-FDi01) that split the light into two channels, with one filter (ET525/50m or HQ580m60) in each channel. The two channels were imaged on the two halves of the EMCCD camera.

Information on single-molecule polymerization was extracted using a home-written MATLAB program from the fluorescence images in the movies, 'iQPALM' (image-based quantitative photo-activated localization microscopy[47,48]), and other codes (Supplementary Software 1). The initial results were further analysed based on the SEM images of the marker particles. More details are provided in Supplementary Section 1.8.

Data availability

All data are available in the main text or the Supplementary Information. Raw data supporting the findings of this study are available upon reasonable request. Source data are provided with this paper.

Code availability

MATLAB codes are included in Supplementary Software 1.

References

44. Herman, T. K., Mackowiak, S. A. & Kaufman, L. J. High power light emitting diode based setup for photobleaching fluorescent impurities. *Rev. Sci. Instrum.* **80**, 016107 (2009).
45. Ng, J. D. et al. Single-molecule investigation of initiation dynamics of an organometallic catalyst. *J. Am. Chem. Soc.* **138**, 3876–3883 (2016).
46. Kozma, I. Z., Krok, P. & Riedle, E. Direct measurement of the group-velocity mismatch and derivation of the refractive-index dispersion for a variety of solvents in the ultraviolet. *J. Opt. Soc. Am. B* **22**, 1479–1485 (2005).
47. Chen, T.-Y. et al. Concentration- and chromosome-organization-dependent regulator unbinding from DNA for transcription regulation in living cells. *Nat. Commun.* **6**, 7445 (2015).
48. Chen, P. & Chen, T.-Y. MATLAB code package: iQPALM (image-based quantitative photo-activated localization microscopy) https://doi.org/10.6084/m9.figshare.12642617.v1 (2020).

Acknowledgements

This research was supported by the Army Research Office (grant no. W911NF-18-1-0217). R.Y. acknowledges support from a Cornell

Presidential Postdoctoral Fellowship. This work made use of the NMR and Chemistry Mass Spectrometry Facilities at Cornell University, which is supported, in part, by the National Science Foundation (NSF) under award CHE-1531632. The research was carried out using Cornell Center for Materials Research Shared Facilities supported by the NSF (grant no. DMR-1719875).

Author contributions

R.Y. improved the experimental design, performed imaging experiments and bulk polymerization, coded software, analysed data and performed simulations. X.S. designed, synthesized and characterized the caged monomers, characterized the monomer uncaging and polymerization reactivity, and performed early imaging experiments. X.M. developed the data analysis pipeline, coded software and analysed data. F.S.A. synthesized and characterized the catalyst labelling reagent. S.B. contributed to the bulk polymerization experiment and NMR characterization. C.L. contributed to early-stage data analysis. G.W.C. contributed to discussions. R.Y. and P.C. wrote the main text. R.Y., X.S., X.M., F.S.A. and P.C. wrote the Supplementary Information. P.C. conceived and directed the research.

Competing interests

Cornell University has filed a US patent application (no. 18/144,022) with P.C., R.Y., X.S. and X.M. as inventors, based on this research, including the methodology and potential applications. The remaining authors declare no competing interests.

Additional information

Supplementary information The online version contains supplementary material available at https://doi.org/10.1038/s41557-023-01363-2.

Correspondence and requests for materials should be addressed to Peng Chen.

Peer review information *Nature Chemistry* thanks Johan Hofkens and the other, anonymous, reviewer for their contribution to the peer review of this work.